Research Square

Preprints are preliminary reports that have not undergone peer review.
They should not be considered conclusive, used to inform clinical practice,
or referenced by the media as validated information.

Dual-Orbital Synergy in Paired Cu(II) Open Metal Sites for Enhanced High-Temperature Hydrogen Isotope Separation

Chuanqin Xia

xiachqin@163.com

Sichuan University

Fenglei Wang

Sichuan University

Zining Wang

Sichuan University

Chaofan Jiang

Sichuan University

Wenting Liu

Sichuan University

Yuchen Jiang

Sichuan University

Yu Luo

Sichuan University

Huimin Li

Sichuan University

Qingyang Wang

Sichuan University

Yuanhua Wang

Sichuan University https://orcid.org/0000-0003-0514-6976

Song Qin

Sichuan University

Yongdong Jin

Sichuan University

Lijian Ma

Sichuan University https://orcid.org/0000-0002-6317-6287

Article

Keywords: Hydrogen isotopes separation, Metal-Organic Frameworks, dual metal open metal sites, confined channel, synergistic effects

Posted Date: October 23rd, 2025

DOI: https://doi.org/10.21203/rs.3.rs-7838780/v1

License: This work is licensed under a Creative Commons Attribution 4.0 International License. Read Full License

Additional Declarations: There is **NO** Competing Interest.

Version of Record: A version of this preprint was published at Nature Communications on August 10th, 2026. See the published version at https://doi.org/10.1038/s41467-026-76556-7.

Abstract

The selective separation of hydrogen isotopes under mild cryogenic conditions remains a formidable challenge due to their nearly identical physicochemical properties. Here, we report a dual strategy of pore topology design and bimetallic synergistic engineering to amplify chemical affinity quantum sieving (CAQS). Among three tailored Cu(II)-MOFs (Cu-bptc, Cu-mbtc, Cu-ATC), Cu-ATC exhibited exceptional performance, achieving a D_2/H_2 selectivity of 20 at 50 K (10 mbar) and 1.8 in breakthrough experiments at 77 K, surpassing all reported Cu-MOFs. The ultramicroporous topology of Cu-ATC fixes a Cu···Cu distance of 5.98 Å within one-dimensional channels (~5.6 Å), while Jahn–Teller distortion induces axial elongation at each Cu(II) center, stabilizing the d_{z^2} orbitals and enhancing their availability for interaction with hydrogen isotope molecules. This dual effect creates two closely spaced open metal sites that can simultaneously interact with H_2 and D_2, amplifying their differential interactions and thereby driving isotope separation via CAQS. The distinct binding strength is evidenced by in situ DRIFTS (H–H stretch red-shift of 682 cm^{-1}) and by DFT calculations showing stronger adsorption of D_2 (−15.8 kJ mol^{-1} at the primary site). These microscopic differences account for the observed D_2/H_2 selectivity, highlighting a new paradigm for CAQS-based isotope separation under mild cryogenic conditions.

INTRODUCTION

Deuterium enrichment from hydrogen isotope mixtures represents a critical bottleneck in nuclear fusion fuel cycles. In current tokamak reactors, the utilization of D_2 and T_2 fuels is typically below 10%, with most discharged as waste streams, leading to tritium loss and the requirement for continuous deuterium enrichment to sustain the fuel cycle. [1,2] Despite decades of research, conventional separation technologies, including cryogenic distillation, thermal diffusion, and chromatographic methods, suffer from high energy consumption and low separation factors (~ 1.5), rendering them economically unsustainable for large-scale implementation, [3] underscoring the urgent need for new approaches that combine higher selectivity with lower energy demand. The intrinsic difficulty in hydrogen isotope separation lies in their nearly identical physicochemical properties, with the primary difference being a mass ratio of two, necessitating the exploitation of quantum effects for efficient separation under mild conditions.

Metal–organic frameworks (MOFs) have emerged as promising platforms for hydrogen isotope separation by exploiting quantum sieving effects arising from zero-point energy differences. [4–7] Kinetic quantum sieving (KQS) can deliver remarkable selectivity—D_2/H_2 = 41.4 at 20 K [8]—through diffusion discrimination in confined pores, but this requires impractically low temperatures. To extend applicability, chemical-affinity quantum sieving (CAQS) was introduced, [9] relying on Kubas-type σ donation and π back-donation between H_2/D_2 and open metal sites. [10–17] At 77 K, however, achieving high selectivity (> 10) remains challenging, particularly regarding stability and capacity for practical application. Building on this, researchers have attempted to combine the two mechanisms. Imidazole-modified MOF-74 achieved

a selectivity of 26 at 77 K, [18] while Cu(I)-exchanged ZSM-5 reached 24.9 at 100 K. [19] These studies illustrate the potential of KQS–CAQS synergy, yet they also highlight persistent challenges including the instability of Cu(I) sites, the complexity of post-synthetic modification, and the rapid loss of selectivity once the temperature rises above 77 K. The central challenge therefore remains to establish isotope–metal interactions that are both strong and durable, capable of sustaining high selectivity under practical cryogenic conditions without compromising framework integrity.

Among MOF architectures, Cu(II)-based paddlewheel frameworks are particularly attractive because their robust [$Cu_2(O_2CR)_4$] secondary building units(SBUs, Fig. 1(c)) allow facile generation of open metal sites upon activation and systematic modulation of pore environments. In addition, the Jahn–Teller distortion intrinsic to Cu(II) enhances the accessibility of d_z^2 orbitals for guest–molecule interactions, [20,21] offering potential advantages for isotope binding. Despite these features, benchmark Cu-BTC (HKUST-1) delivers only modest performance, with a D_2/H_2 selectivity of 1.3 at 77 K, [22–27] as its large ~ 1 nm cages permit molecules to bypass OMSs and diminish the CAQS effect. Attempts to improve performance by reducing Cu(II) to Cu(I) temporarily boosted selectivity to 37.9 at 30 K, [28] but this advantage quickly disappeared above 40 K because the reduction disrupted d_z^2 orbital alignment and undermined framework stability. A similar issue was observed in FJI-Y11, [29] where DFT calculations revealed that adsorption occurred near oxygen atoms rather than Cu centers, as the d_z^2 orbitals were geometrically misaligned with the pore channels, limiting effective interaction with hydrogen molecules and resulting in low selectivity ($\alpha \approx 1.4$).

These observations show that OMS density alone is not sufficient, and that isotope separation critically depends on how pore confinement and orbital orientation cooperate. A promising direction is therefore to design frameworks with ultramicroporous channels that enforce close contact between isotopes and appropriately oriented, Jahn–Teller–stabilized Cu(II) sites, while preserving the structural integrity of the paddlewheel motif.

Guided by this rationale, we synthesized three tetracarboxylate Cu(II) MOFs with distinct topologies including cage-type Cu-bptc, [30] wide-channel Cu-mbtc (~ 10 Å), [31] and ultramicroporous Cu-ATC (~ 5 Å), [32] to examine how pore architecture affects isotope separation. Comparative evaluation showed that Cu-bptc and Cu-mbtc displayed only limited selectivity, indicating that pore confinement alone cannot account for high performance. In contrast, Cu-ATC exhibited outstanding separation, achieving a D_2/H_2 selectivity of 20 at 50 K and 1.8 in breakthrough experiments at 77 K, surpassing all reported Cu(II) MOFs. Subsequent analysis revealed that its ultramicroporous channels not only constrain molecular motion but also position isotopes within reach of two closely spaced paddlewheel Cu(II) sites, where accessible d_z^2 orbitals enable cooperative dual-site interactions that markedly amplify the CAQS effect. These findings establish Cu-ATC as a benchmark system and highlight a generalizable design principle in which pore topology and site-specific electronic structure act in concert to realize practical hydrogen isotope separation under mild cryogenic conditions.

RESULTS AND DISCUSSIONS

Structure Characterization

The structures of the three Cu(II)-based MOFs were characterized by powder X-ray diffraction (PXRD) and nitrogen adsorption-desorption experiments, with detailed results provided in the Supporting Information. The PXRD patterns confirmed that the crystal structures of these materials aligned with literature reports, indicating successful synthesis and high purity (Figure S1-3). The nitrogen adsorption isotherms exhibited IUPAC Type I characteristics for all three MOFs, verifying their microporous nature (Figure S4-6). Pore size distributions (Figure S7-9), calculated using nonlocal density functional theory (NLDFT), revealed distinct topologies: Cu-ATC and Cu-bptc possess narrow ultramicropore (5.6 Å and 5.8 Å, respectively), whereas Cu-mbtc showed a larger pore size (10.0 Å). This variation reflects the designed optimization from cage-like Cu-bptc to one-dimensional channels in Cu-mbtc and Cu-ATC (Fig. 1). Brunauer-Emmett-Teller (BET) surface areas were 606 $m^2 g^{-1}$ for Cu-ATC, 1811 $m^2 g^{-1}$ for Cu-bptc, and 498 $m^2 g^{-1}$ for Cu-mbtc (Figure S4-6). These values correlate with framework compactness: Cu-bptc's high surface area arises from its interconnected cage network, whereas Cu-ATC's lower value stems from denser ultramicroporous channels. Such topological tuning establishes the structural basis for subsequent hydrogen isotope adsorption studies, consistent with the dual strategy of pore topology modulation and bimetallic synergy.

Adsorption properties of H_2 and D_2

Single-component H_2 and D_2 adsorption isotherms for the three MOFs were measured at 77 K and 87 K (Fig. 2a,b). At 77 K and 101 kPa, Cu-bptc exhibited high uptake capacities (q): 248.907 $cm^3 g^{-1}$ for D_2 and 219.596 $cm^3 g^{-1}$ for H_2, outperforming many reported MOF-based hydrogen storage materials. In contrast, Cu-ATC showed lower capacities (154.2 $cm^3 g^{-1}$ for D_2 and 146.6 $cm^3 g^{-1}$ for H_2), attributable to its narrow one-dimensional channels (~ 5.6 Å) limiting accessible volume, while Cu-bptc's cage-like structure (~ 8–10 Å) offers larger voids. Cu-mbtc displayed even lower uptakes (85.6 $cm^3 g^{-1}$ for D_2 and 76.8 $cm^3 g^{-1}$ for H_2), despite a comparable surface area to Cu-ATC, highlighting the adverse effect of channel expansion (~ 10 Å) in topologically similar frameworks.

To evaluate the adsorption density of hydrogen isotope molecules on the surface of MOFs, BET surface area-normalized capacities (q_{SA}, $q_{SA}=q/S_{BET}$) were calculated (Fig. 2c). At 77 K, Cu-ATC's q_{SA} values (0.257 $cm^3 m^{-2}$ for D_2 and 0.244 $cm^3 m^{-2}$ for H_2) were approximately twice those of Cu-bptc (0.136 $cm^3 m^{-2}$ for D_2 and 0.120 $cm^3 m^{-2}$ for H_2) and Cu-mbtc (0.154 $cm^3 m^{-2}$ for D_2 and 0.172 $cm^3 m^{-2}$ for H_2), demonstrating superior adsorption utilization per unit area in Cu-ATC's ultramicroporous topology, despite its lower absolute capacity. The isotherm steepness in the low-pressure region (< 10 kPa at 77 K) followed the order Cu-ATC > Cu-bptc > Cu-mbtc (Fig. 2a), reflecting stronger gas-framework interactions and faster adsorption kinetics in Cu-ATC. At 87 K (Fig. 2b), Cu-ATC's capacities decreased by only 8–9% (at 101 kPa), whereas Cu-bptc and Cu-mbtc decreased by 25–28% and 36–37%, respectively, underscoring Cu-ATC's enhanced adsorption stability at elevated temperatures.

Ideal adsorbed solution theory (IAST) selectivity for D_2/H_2 (equimolar mixture), computed using a dual-site Langmuir-Freundlich model, was 1.84 for Cu-ATC at 77 K, surpassing those of Cu-bptc (1.42) and Cu-mbtc (1.42). At 87 K, Cu-ATC retained 1.60, while the others dropped to 1.17 and 1.38. These results affirm Cu-ATC's superior separation performance under mild conditions.

Isosteric heats of adsorption (Q_{st}), derived via the virial method (Fig. 2d), further elucidated the mechanism. Cu-ATC's zero-coverage Q_{st} values were 12.47 kJ mol^{-1} for D_2 and 12.09 kJ mol^{-1} for H_2—the highest among copper paddlewheel MOFs—exceeding those of Cu-bptc (7.26/6.70 kJ mol^{-1}), Cu-mbtc (7.26/6.88 kJ mol^{-1}), FJI-Y11 (7.88/7.13 kJ mol^{-1}), and HKUST-1 (7.32/6.41 kJ mol^{-1}). Cu-ATC also outperformed Co-MOF-74 (12.1/11.0 kJ mol^{-1}) and Zn-MOF-74 (9.2/8.3 kJ mol^{-1}), being only slightly below Ni-MOF-74 (13.7/12.1 kJ mol^{-1}). The maximum D_2-H_2 Q_{st} difference of 1.4 kJ mol^{-1} ranks among the highest for copper paddlewheel MOFs, indicating that paired OMSs and ultramicropores synergistically enhance isotope affinity differences, bolstering the CAQS mechanism.

In Situ Diffuse Reflectance Infrared Fourier Transform Spectroscopy (DRIFTS)

To probe the H_2 adsorption mechanism in the MOFs, a stepwise hydrogen dosing protocol (2.6 mL min^{-1} per dose) was employed with *In situ* DRIFTS monitoring at room temperature (298 K) (Fig. 3). In Cu-ATC, increasing H_2 exposure produced a progressively intensified broad absorption band centered at 3479 cm^{-1}, red-shifted by 682 cm^{-1} relative to free H_2 vibrations (~ 4161 cm^{-1}). [33,34] This substantial shift confirms a strong interaction between H_2 and OMSs, supporting dihydrogen bond formation even at ambient temperature. In contrast, Cu-bptc and Cu-mbtc showed no detectable H_2-related IR signals (Fig. 3b and c), indicating negligible chemisorption at 298 K. This observation is consistent with Cu-ATC's elevated adsorption enthalpies (Q_{st} >12 kJ mol^{-1}), highlighting topological differences: Cu-ATC's ultramicroporous one-dimensional channels (~ 5.6 Å) facilitate optimized H_2 interactions with paired OMSs (symmetric d_z^2 orbitals), whereas the larger cavities/channels (> 8 Å) in Cu-bptc and Cu-mbtc allow molecules to bypass OMSs, weakening the interaction. These DRIFTS results directly substantiate Cu-ATC's CAQS advantage through structural synergy, extending the applicability of copper paddlewheel MOFs under mild conditions.

Cryogenic Thermal Desorption Spectroscopy (TDS): Adsorption Sites and Isotope Preferential Binding

To identify adsorption sites in the three MOFs and their affinity for H_2/D_2, TDS measurements were conducted. Samples were exposed to an equimolar H_2/D_2 mixture (10 mbar) at 26 K for 10 min, evacuated to 20 K, and heated at 0.1 K s^{-1} (6 K min^{-1}) over 20–150 K (Fig. 4). Cu-ATC's TDS spectrum revealed two desorption peaks (Fig. 4a): a higher-temperature peak assigned to OMSs (Site I) and a lower-temperature peak associated with framework oxygen atoms (Site II). D_2 peaks shifted to higher temperatures than H_2, indicating preferential D_2 binding at OMSs due to lower zero-point energy, thereby enhancing CAQS, consistent with the Q_{st} difference (1.4 kJ mol^{-1}) and DRIFTS redshift. Cu-bptc showed

three peaks (Fig. 4c): OMSs (I), oxygen atoms (II), and small pores (III), but with smaller D_2/H_2 shifts, reflecting diluted site-specific interactions in its cage-like topology. Cu-mbtc exhibited two peaks (Fig. 4e): OMSs (I) and large pores (II), with the weakest D_2 preference, attributed to channel expansion (~ 10 Å) diminishing interactions. These TDS results quantify topology-dependent site diversity: Cu-ATC's ultramicroporous channels amplify OMS preference for D_2 (largest peak shift), providing the basis for its high selectivity and distinguishing it from conventional copper MOFs.

Separation Performance

To assess the practical impact of the MOF topologies on separation, samples were exposed to an equimolar H_2/D_2 mixture (10 mbar) at varying temperatures (26, 50, 77, 87 K), with selectivity ($S_{D2/H2}$ = D_2/H_2 desorption area ratio) evaluated via TDS (Fig. 5 and Supporting Information Figures S10–12). At 26 K, all adsorption sites (strong and weak) were occupied, and the combined KQS and CAQS effects yielded a high D_2 preference. Above 50 K, adsorption was confined to OMSs, yet CAQS continued to favor D_2. Cu-bptc and Cu-mbtc selectivities declined sharply with temperature, reflecting their weak OMS affinity, whereas Cu-ATC exhibited superior values: 20 at 50 K (the highest among all tested Cu(Ⅱ)-MOFs) and 8.0 at 87 K. This performance originates from its ultramicroporous channels (~ 5.6 Å) and paired OMS synergy enhancing isotope affinity differences, consistent with Q_{st} and DRIFTS results. These findings underscore Cu-ATC's CAQS potential above liquid nitrogen temperatures, supporting its promise for industrial hydrogen isotope separation (Fig. 6).

Dynamic column breakthrough experiments

To simulate industrial H_2/D_2 separation, dynamic column breakthrough experiments were performed using an H_2/D_2/Ne mixture (10/10/80 vol.%) at a flow rate of 5 mL min^{-1}, 77 K, and 100 kPa (Fig. 7). In all materials, H_2 broke through first (reflecting its lower binding affinity), whereas D_2 was retained longer. Cu-mbtc showed nearly simultaneous H_2/D_2 breakthrough (Fig. 7c), yielding a low selectivity of 1.35, due to channel dilation that weakens isotope discrimination separation. In contrast, Cu-ATC exhibited an H_2 breakthrough time of 823 s g^{-1} (Fig. 7a), much shorter than Cu-bptc's 2593 s g^{-1} (Fig. 7b), reflecting accelerated displacement kinetics in its ultramicroporous framework. For D_2, the breakthrough time was 5400 s g^{-1} in Cu-ATC, significantly longer than that of Cu-bptc (2483 s g^{-1}), demonstrating enhanced retention. Curve integration yielded dynamic parameters: Cu-ATC showed a D_2 capacity of 1.04 mmol g^{-1} with a selectivity of 1.8, outperforming Cu-bptc (1.2) and Cu-mbtc (1.35). Although dynamic values were lower than those from static isotherms, owing to incomplete equilibration under flow, Cu-ATC's performance corroborates its industrial potential, consistent with its TDS selectivity (20 at 50 K).

Adsorption mechanism study

To elucidate the hydrogen adsorption and separation mechanisms in the three MOFs, Grand Canonical Monte Carlo (GCMC) simulations were conducted in Materials Studio at 77 K and constant pressure and probability density maps of H_2 were obtained as shown in Fig. 8, the results showed two primary

adsorption sites in Cu-ATC (Fig. 8a): (I) near copper paddlewheel OMSs and (II) proximal to oxygen atoms in the clusters. Adsorption at Site II was attributed to the compact structure, which facilitated significant interactions between H_2 and oxygen atoms within the framework. In contrast, Cu-bptc (Fig. 8b) exhibited uniform H_2 distribution across cage-like cavities, lacking OMS localization; its spacious voids (~ 8–10 Å) dilute interactions, weakening the CAQS effect. Cu-mbtc (Fig. 8c) showed a preference for wall-bound OMSs due to the excessively large pore size (~ 10 Å). The above three patterns confirm topological control: Cu-ATC's confined channels (~ 5.6 Å) enforce OMS engagements, boosting CAQS.

Periodic density functional theory (DFT) calculations, based on GCMC-identified sites, assessed H_2 adsorption energies (Fig. 9). Cu-ATC's primary Site I (between adjacent paddlewheels) yielded a H_2 adsorption energy of -11.01 kJ mol^{-1}, matching experimental Q_{st}, far stronger than the values at the comparable OMS in Cu-bptc (-8.52 kJ mol^{-1}) and Cu-mbtc (-7.30 kJ mol^{-1}). This enhancement arises from Cu-ATC's short Cu-Cu distance (5.98 Å). As shown in Fig. 10a, the charge density difference (CDD) calculated using vaspkit further demonstrates that D_2 simultaneously engages in strong synergistic orbital interactions with the facing Cu d_{Z^2} orbitals in Cu-ATC, the calculated binding energy for this interaction was as high as -15.8 kJ mol^{-1}. Integrated analyses reveal key structural determinants: although Cu-ATC and Cu-bptc share similar apertures, Cu-bptc's oversized cages and OMS-diffusion path mismatch limit interactions to single OMSs. Cu-mbtc's dilated channels hinder d_z^2 orbital engagement. Conversely, Cu-ATC's ultramicropores synergize three features: (i) optimal vacant d_z^2 orbital alignment along diffusion trajectories, (ii) confined spaces promote the trapping of hydrogen isotope molecules by OMS, and (iii) proximate OMS spacing for dual-site cooperativity. These enable rapid, simultaneous dual-OMS engagements, accelerating and intensifying isotope interactions to amplify CAQS, conferring superior H_2/D_2 separation even at 77 K and positioning Cu-ATC as an innovative benchmark in stable Cu(II)-MOFs.

CONCLUSION

In summary, we demonstrate that pore topology modulation combined with bimetallic synergistic engineering enables Cu-ATC, a paddlewheel-type MOF with one-dimensional ultramicroporous channels, to achieve record hydrogen isotope separation performance. Cu-ATC exhibits steep adsorption isotherms at low pressures and a TDS selectivity of 20 at 50 K, the highest among reported Cu(II)-MOFs. Importantly, at 77 K, its dynamic breakthrough selectivity of 1.8 is maintained, arising from synergistic interactions between paired Cu sites and ~ 5.6 Å channels that amplify CAQS (ΔQ_{st}= 1.4 kJ mol^{-1}). These findings establish the structural principles by which confinement and OMS arrangement cooperate to determine isotope separation, providing a general framework for designing efficient MOFs under mild conditions and advancing deuterium enrichment technologies.

Declarations

ASSOCIATED CONTENT

Supporting Information: XRD patterns of samples. Experimental details. GCMC and DFT calculation details. Thermal desorption spectra of samples. Summary of hydrogen isotope separation factors for various porous frameworks.

AUTHOR INFORMATION

Corresponding Authors:

Chuanqin Xia- College of Chemistry, Sichuan University, Chengdu 610064, P.R. China. E-mail: xiachqin@163.com

Lijian Ma- College of Chemistry, Sichuan University, Chengdu 610064, P.R. China. E-mail: ma.lj@hotmail.com

Notes: The authors declare no competing financial interest.

Acknowledgments: This work was supported by the National Natural Science Foundation of China (Grant No. 22176136, U21A20296, 22376149，U1867205), and the Key Research and Development Program of Sichuan Province, China (Project No. 2020YFS0070, 2021YFH0170). We are grateful for the technical support from the Comprehensive Training Platform of the Specialized Laboratory (College of Chemistry, Sichuan University) and Analytical & Testing Center of Sichuan University.

References

1. Glugla, M. *et al.* ITER fuel cycle R&D: Consequences for the design. *Fusion Engineering and Design* **81**, 733-744, doi:https://doi.org/10.1016/j.fusengdes.2005.07.038 (2006).
2. Smith, R. *et al.* Hydrogen isotope separation for fusion power applications. *Journal of Alloys and Compounds* **645**, S51-S55, doi:https://doi.org/10.1016/j.jallcom.2015.01.231 (2015).
3. Rae, H. K. in *Separation of Hydrogen Isotopes* Vol. 68 *ACS Symposium Series* Ch. 1, 1-26 (AMERICAN CHEMICAL SOCIETY, 1978).
4. Gao, L. G., Zhang, R. M., Xu, X. & Truhlar, D. G. Quantum Effects on H2 Diffusion in Zeolite RHO: Inverse Kinetic Isotope Effect for Sieving. *Journal of the American Chemical Society* **141**, 13635-13642, doi:10.1021/jacs.9b06506 (2019).
5. Perez-Carbajo, J., Parra, J. B., Ania, C. O., Merkling, P. J. & Calero, S. Molecular Sieves for the Separation of Hydrogen Isotopes. *ACS Applied Materials & Interfaces* **11**, 18833-18840, doi:10.1021/acsami.9b02736 (2019).
6. Zhang, L. *et al.* Exploiting Dynamic Opening of Apertures in a Partially Fluorinated MOF for Enhancing H2 Desorption Temperature and Isotope Separation. *Journal of the American Chemical Society* **141**, 19850-19858, doi:10.1021/jacs.9b10268 (2019).

7. Zhao, F.-J., Tan, Y.-X., Wang, W., Ju, Z. & Yuan, D. Optimizing H2, D2, and C2H2 Sorption Properties by Tuning the Pore Apertures in Metal–Organic Frameworks. *Inorganic Chemistry* **57**, 13312-13317, doi:10.1021/acs.inorgchem.8b01864 (2018).
8. Cao, D. *et al.* Ultrahigh effective H2/D2 separation in an ultramicroporous metal–organic framework material through quantum sieving. *Journal of Materials Chemistry A* **6**, 19954-19959, doi:10.1039/C8TA05707A (2018).
9. FitzGerald, S. A., Pierce, C. J., Rowsell, J. L. C., Bloch, E. D. & Mason, J. A. Highly Selective Quantum Sieving of D2 from H2 by a Metal–Organic Framework As Determined by Gas Manometry and Infrared Spectroscopy. *Journal of the American Chemical Society* **135**, 9458-9464, doi:10.1021/ja402103u (2013).
10. Belkova, N. V., Epstein, L. M., Filippov, O. A. & Shubina, E. S. Hydrogen and Dihydrogen Bonds in the Reactions of Metal Hydrides. *Chemical Reviews* **116**, 8545-8587, doi:10.1021/acs.chemrev.6b00091 (2016).
11. Crabtree, R. H. Dihydrogen Complexation. *Chemical Reviews* **116**, 8750-8769, doi:10.1021/acs.chemrev.6b00037 (2016).
12. Georgiev, P. A. & Albinati, A. Nonclassical hydrides of Ni+ in ZSM-5 zeolite structures: A hybrid DFT study. *Chemical Physics Letters* **545**, 66-70, doi:https://doi.org/10.1016/j.cplett.2012.07.019 (2012).
13. Georgiev, P. A., Albinati, A., Mojet, B. L., Ollivier, J. & Eckert, J. Observation of Exceptionally Strong Binding of Molecular Hydrogen in a Porous Material: Formation of an η2-H2 Complex in a Cu-Exchanged ZSM-5 Zeolite. *Journal of the American Chemical Society* **129**, 8086-8087, doi:10.1021/ja072240l (2007).
14. Grubbs, G. S., Obenchain, D. A., Pickett, H. M. & Novick, S. E. J. T. J. o. C. P. H2—AgCl: A spectroscopic study of a dihydrogen complex. **141** (2014).
15. Kubas, G. J. Breaking the H2 Marriage and Reuniting the Couple. *Science* **314**, 1096-1097, doi:10.1126/science.1135430 (2006).
16. Kubas, G. J. Fundamentals of H2 Binding and Reactivity on Transition Metals Underlying Hydrogenase Function and H2 Production and Storage. *Chemical Reviews* **107**, 4152-4205, doi:10.1021/cr050197j (2007).
17. Kubas, G. J., Ryan, R. R., Swanson, B. I., Vergamini, P. J. & Wasserman, H. J. Characterization of the first examples of isolable molecular hydrogen complexes, M(CO)3(PR3)2(H2) (M = molybdenum or tungsten; R = Cy or isopropyl). Evidence for a side-on bonded dihydrogen ligand. *Journal of the American Chemical Society* **106**, 451-452, doi:10.1021/ja00314a049 (1984).
18. Kim, J. Y. *et al.* Exploiting Diffusion Barrier and Chemical Affinity of Metal–Organic Frameworks for Efficient Hydrogen Isotope Separation. *Journal of the American Chemical Society* **139**, 15135-15141, doi:10.1021/jacs.7b07925 (2017).
19. Xiong, R. *et al.* Highly effective hydrogen isotope separation through dihydrogen bond on Cu(I)-exchanged zeolites well above liquid nitrogen temperature. *Chemical Engineering Journal* **391**, 123485, doi:https://doi.org/10.1016/j.cej.2019.123485 (2020).

20. Alzahrani, K. A. H. & Deeth, R. J. Density functional calculations reveal a flexible version of the copper paddlewheel unit: implications for metal organic frameworks. *Dalton Transactions* **45**, 11944-11948, doi:10.1039/C6DT01474G (2016).
21. Deeth, R. J. & Gerloch, M. Ligand-field parameters and the stereochemical activity of d shells in trigonal-bipyramidal complexes of the first transition series. *Inorganic Chemistry* **24**, 4490-4493, doi:10.1021/ic00220a014 (1985).
22. Krawiec, P. *et al.* Improved Hydrogen Storage in the Metal-Organic Framework Cu3(BTC)2. *Advanced Engineering Materials* **8**, 293-296, doi:https://doi.org/10.1002/adem.200500223 (2006).
23. Lee, J., Li, J. & Jagiello, J. Gas sorption properties of microporous metal organic frameworks. *Journal of Solid State Chemistry* **178**, 2527-2532, doi:https://doi.org/10.1016/j.jssc.2005.07.002 (2005).
24. Panella, B., Hirscher, M., Pütter, H. & Müller, U. Hydrogen Adsorption in Metal–Organic Frameworks: Cu-MOFs and Zn-MOFs Compared. *Advanced Functional Materials* **16**, 520-524, doi:https://doi.org/10.1002/adfm.200500561 (2006).
25. Rowsell, J. L. C. & Yaghi, O. M. Effects of Functionalization, Catenation, and Variation of the Metal Oxide and Organic Linking Units on the Low-Pressure Hydrogen Adsorption Properties of Metal–Organic Frameworks. *Journal of the American Chemical Society* **128**, 1304-1315, doi:10.1021/ja056639q (2006).
26. Wong-Foy, A. G., Matzger, A. J. & Yaghi, O. M. Exceptional H2 Saturation Uptake in Microporous Metal–Organic Frameworks. *Journal of the American Chemical Society* **128**, 3494-3495, doi:10.1021/ja058213h (2006).
27. Xiao, B. *et al.* High-Capacity Hydrogen and Nitric Oxide Adsorption and Storage in a Metal–Organic Framework. *Journal of the American Chemical Society* **129**, 1203-1209, doi:10.1021/ja066098k (2007).
28. Hu, X. *et al.* Highly Effective H2/D2 Separation within the Stable Cu(I)Cu(II)-BTC: The Effect of Cu(I) Structure on Quantum Sieving. *ACS Applied Materials & Interfaces* **15**, 3941-3952, doi:10.1021/acsami.2c18221 (2023).
29. Si, Y. *et al.* Highly effective H2/D2 separation in a stable Cu-based metal-organic framework. *Nano Research* **14**, 518-525, doi:10.1007/s12274-019-2571-9 (2021).
30. Chen, B., Ockwig, N. W., Millward, A. R., Contreras, D. S. & Yaghi, O. M. High H2 Adsorption in a Microporous Metal–Organic Framework with Open Metal Sites. *Angewandte Chemie International Edition* **44**, 4745-4749, doi:https://doi.org/10.1002/anie.200462787 (2005).
31. Ma, L., Jin, A., Xie, Z. & Lin, W. Freeze Drying Significantly Increases Permanent Porosity and Hydrogen Uptake in 4,4-Connected Metal–Organic Frameworks. *Angewandte Chemie International Edition* **48**, 9905-9908, doi:https://doi.org/10.1002/anie.200904983 (2009).
32. Chen, B. *et al.* Cu2(ATC)·6H2O: Design of Open Metal Sites in Porous Metal–Organic Crystals (ATC: 1,3,5,7-Adamantane Tetracarboxylate). *Journal of the American Chemical Society* **122**, 11559-11560, doi:10.1021/ja003159k (2000).

33. FitzGerald, S. A., Mukasa, D., Rigdon, K. H., Zhang, N. & Barnett, B. R. Hydrogen Isotope Separation within the Metal–Organic Framework Cu(I)-MFU-4l. *The Journal of Physical Chemistry C* **123**, 30427-30433, doi:10.1021/acs.jpcc.9b09332 (2019).
34. Serykh, A. I. & Kazansky, V. B. Unusually strong adsorption of molecular hydrogen on Cu+ sites in copper-modified ZSM-5. *Physical Chemistry Chemical Physics* **6**, 5250-5255, doi:10.1039/B409848J (2004).

Figures

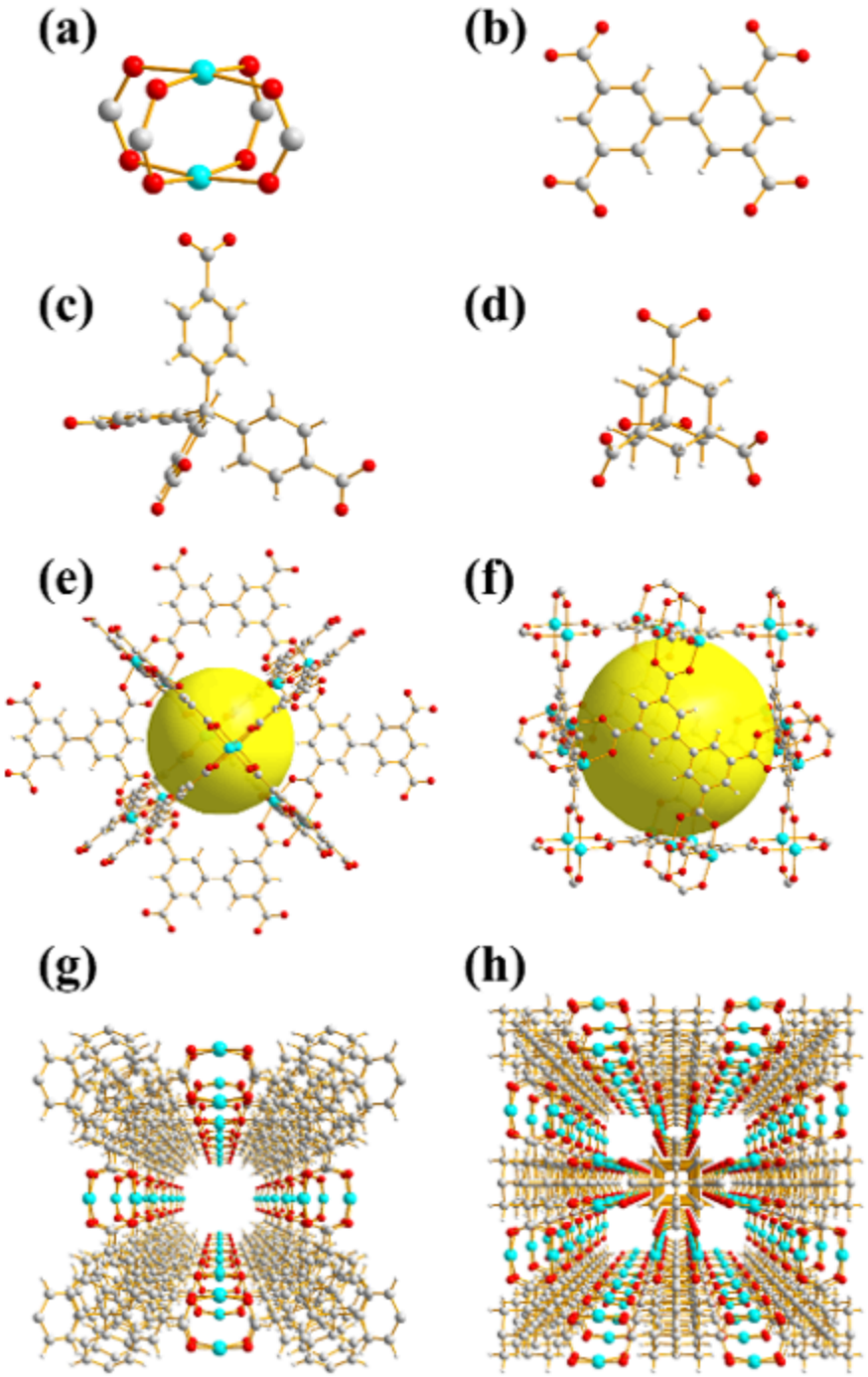

Figure 1

Illustrated structure of (a) $Cu_2(CO_2)_4$ units; (b) 3,3',5,5'-biphenyltetracarboxylate ; (c) 4,4',4",4"'-methanetetrayltetrabenzoate; (d) 1,3,5,7-adamantanetetracarboxylate ; (e) (f) Schematic illustrations of two cage-like structures in Cu-bptc; Three-dimensional structural schematic of (g) Cu-mbtc and (h) Cu-ATC.Atom colors: C: gray, O: red, Cu: cyan, H: white, and the yellow sphere represents the largest sphere that would occupy the cavity without contacting the interior van der Waals surface

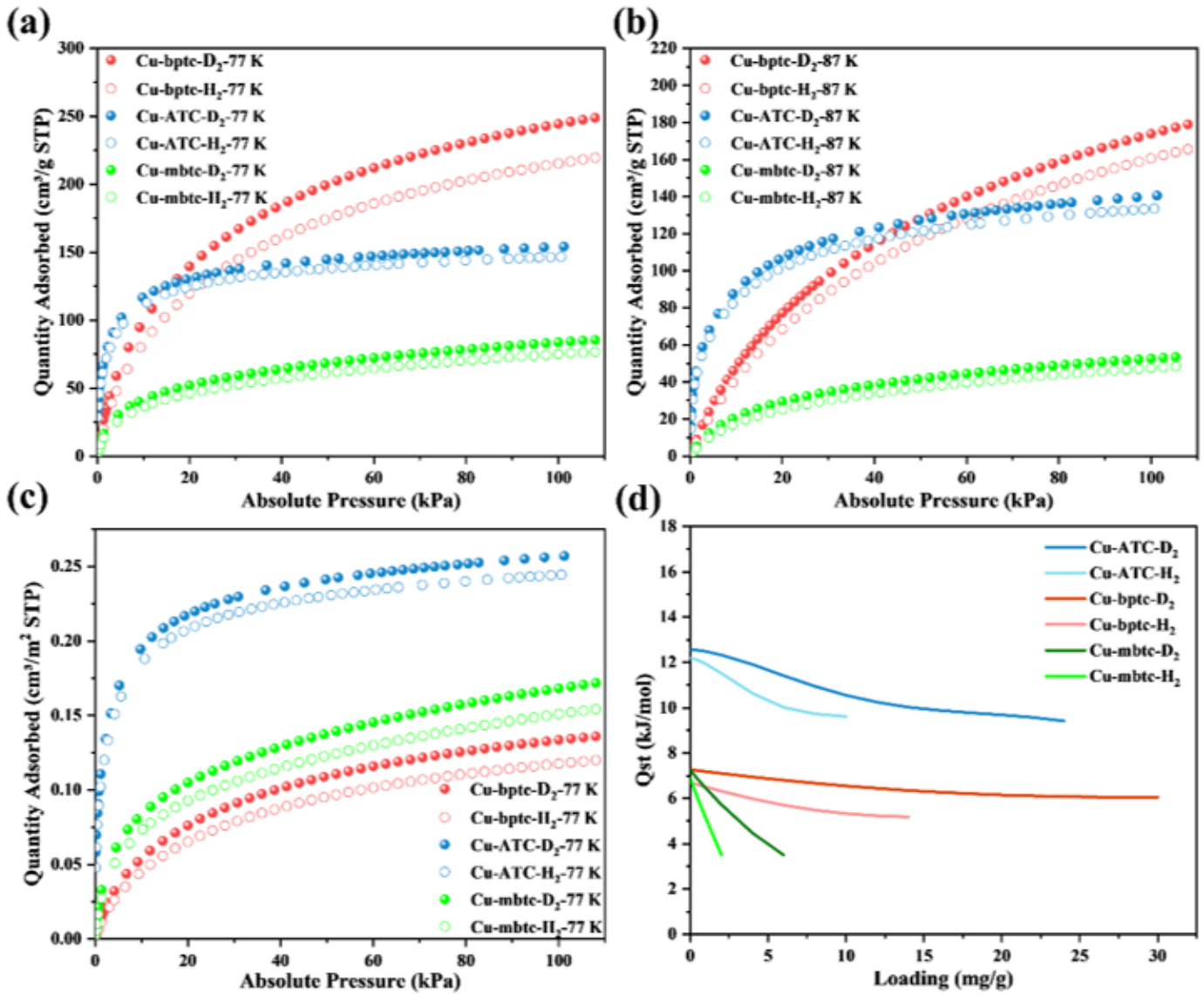

Figure 2

Single-component H_2 and D_2 adsorption isotherms of Cu-ATC (blue), Cu-bptc (red), and Cu-mbtc (green) at 77 K (a) and 87 K (b). Single-component H_2 and D_2 isotherms based on unit BET surface area for Cu-ATC, Cu-bptc, and Cu-mbtcat 77 K (c). The isosteric heat of D_2 and H_2 for Cu-ATC, Cu-bptc, and Cu-mbtc (d).

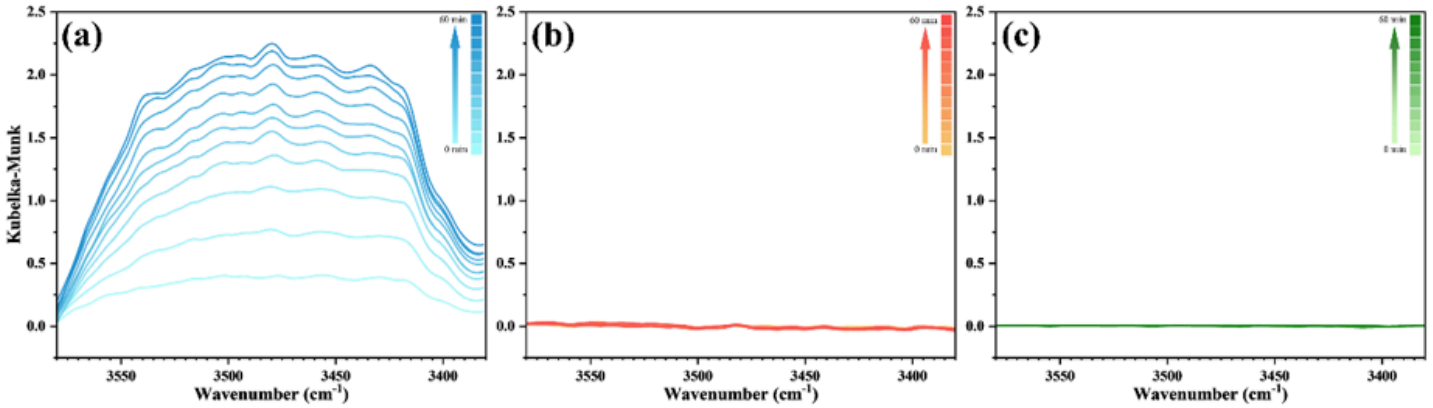

Figure 3

In situ DRIFT spectra of pure H_2 adsorption on Cu-ATC (a), Cu-bptc (b), and Cu-mbtc (c) dosing at 298 K with each dosage being 2.6 mL/min.

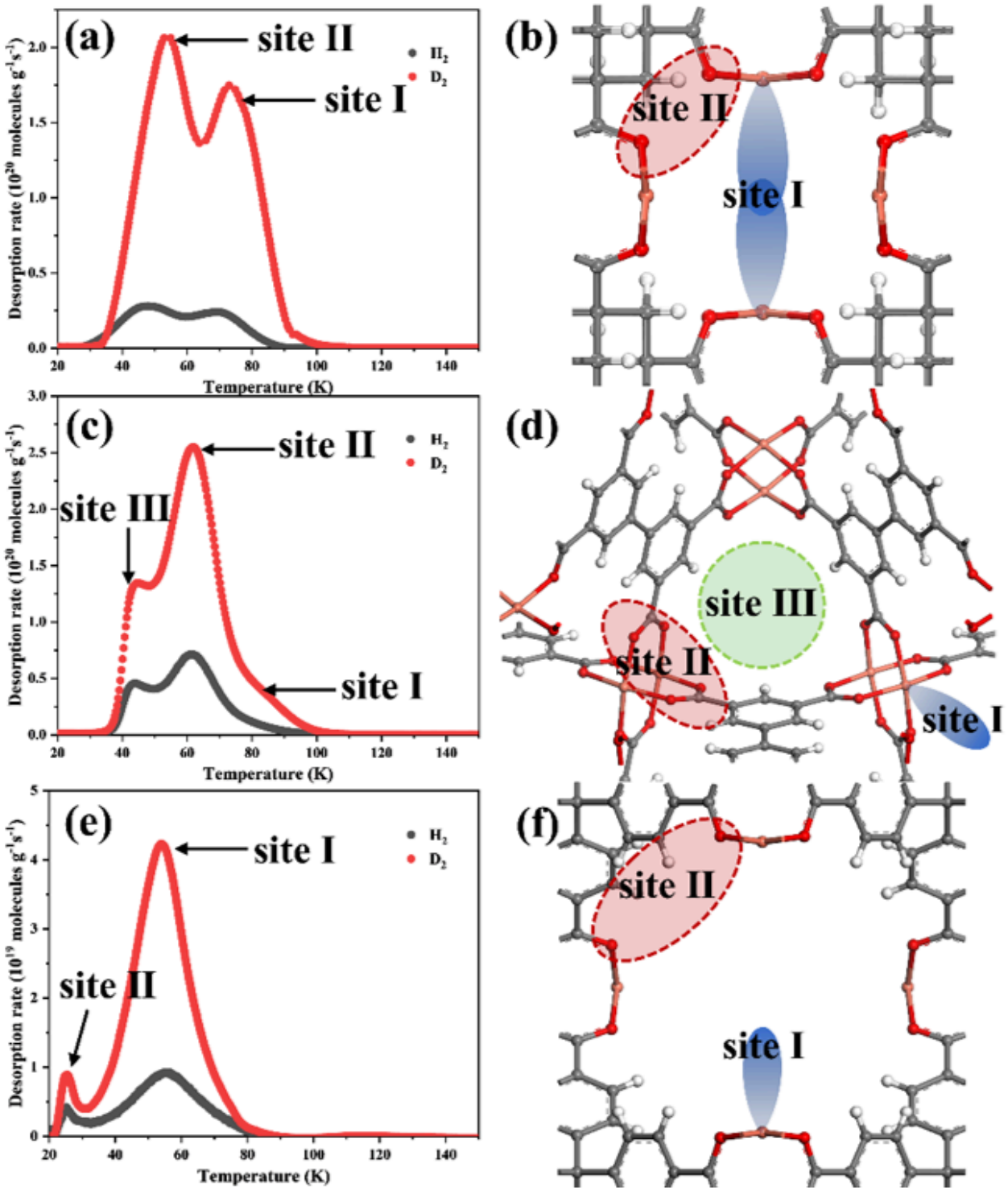

Figure 4

Thermal desorption spectra and corresponding adsorption sites of Cu-ATC (a) (b), Cu-bptc (c) (d), and Cu-mbtc (e) (f). The samples were exposed to 1:1 D_2/H_2 mixture gas at 26 K for 10 min and then evacuated before heating at a rate of 6 K/min.

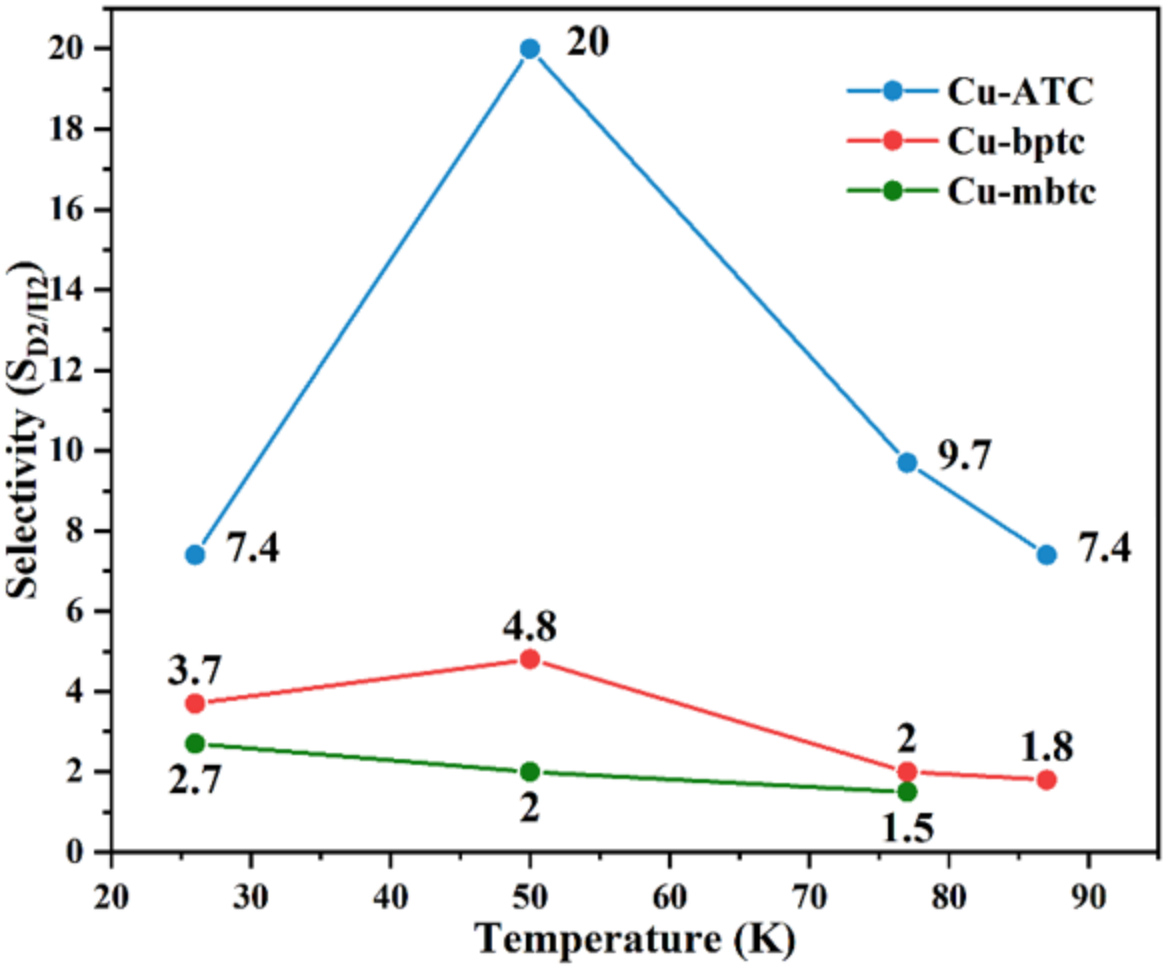

Figure 5

Adsorptive separation for an equimolar D_2/H_2 isotope mixture.

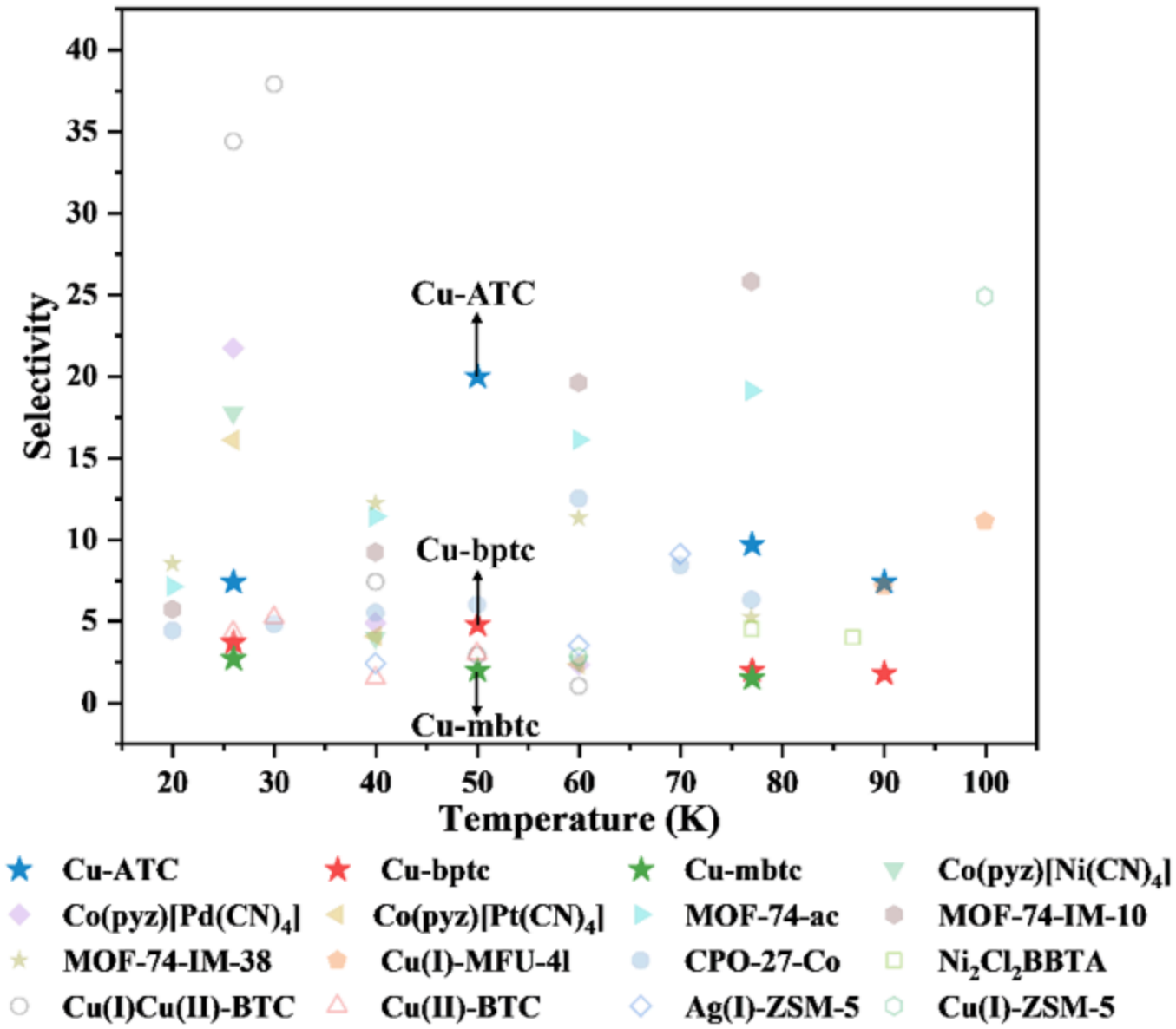

Figure 6

Comparison of the D_2/H_2 selectivity between the results in the literature and our work.

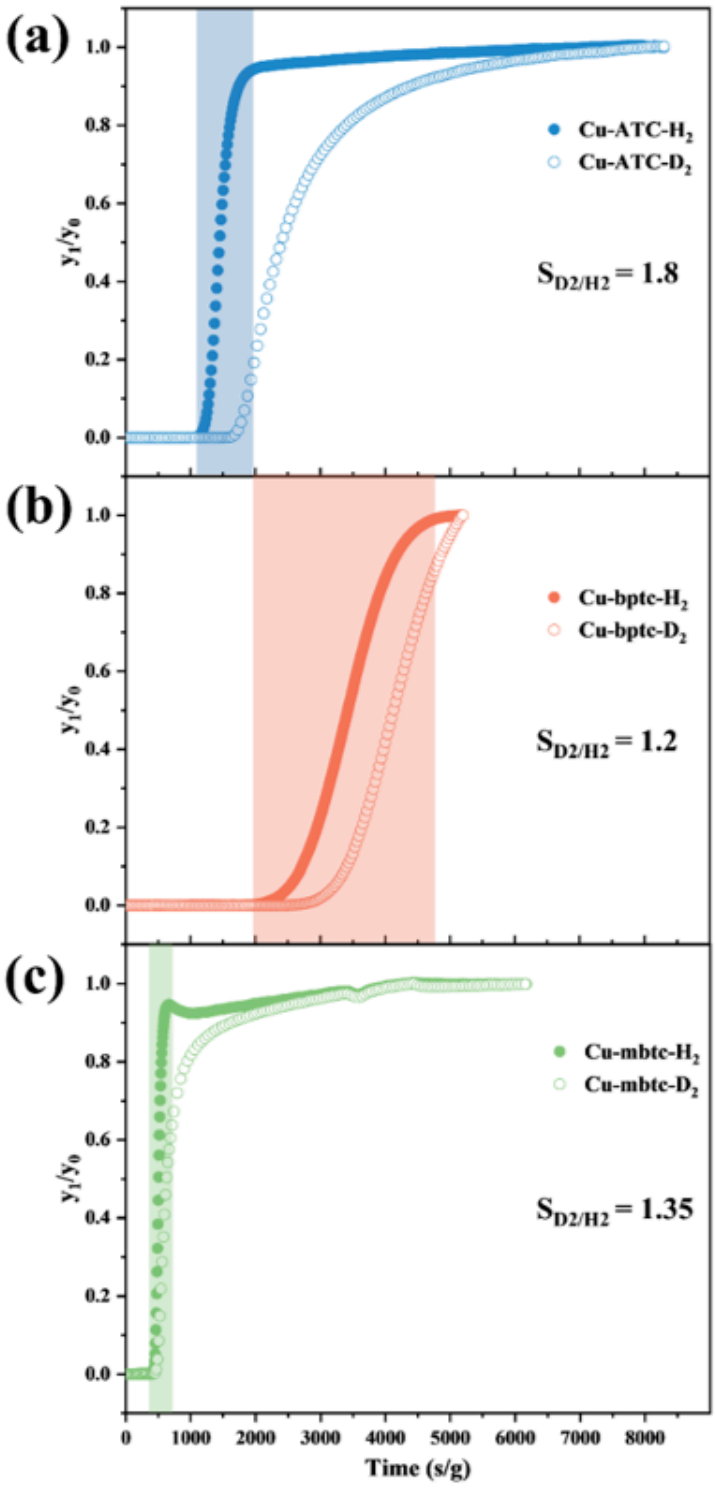

Figure 7

The dynamic breakthrough curves of Cu-ATC (a), Cu-bptc (b), and Cu-mbtc (c) at 77 K for the mixed gases of H_2/D_2/Ne (10/10/80 vol.%).

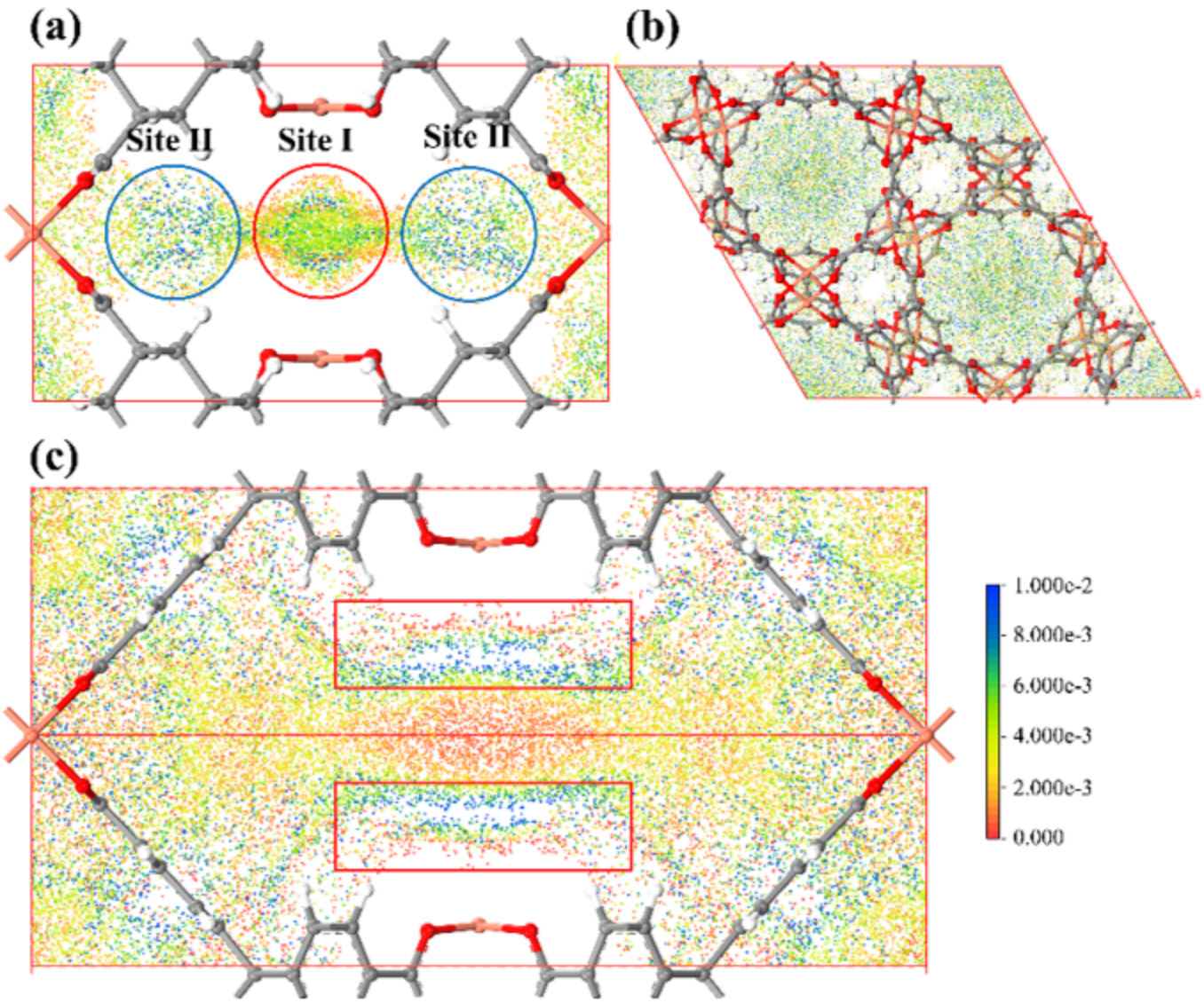

Figure 8

The probability distribution density diagram of H_2 molecules adsorption sites around the Cu-ATC (a), Cu-bptc (b), and Cu-mbtc (c). Color code: C, gray; O, red; Cu, orange.

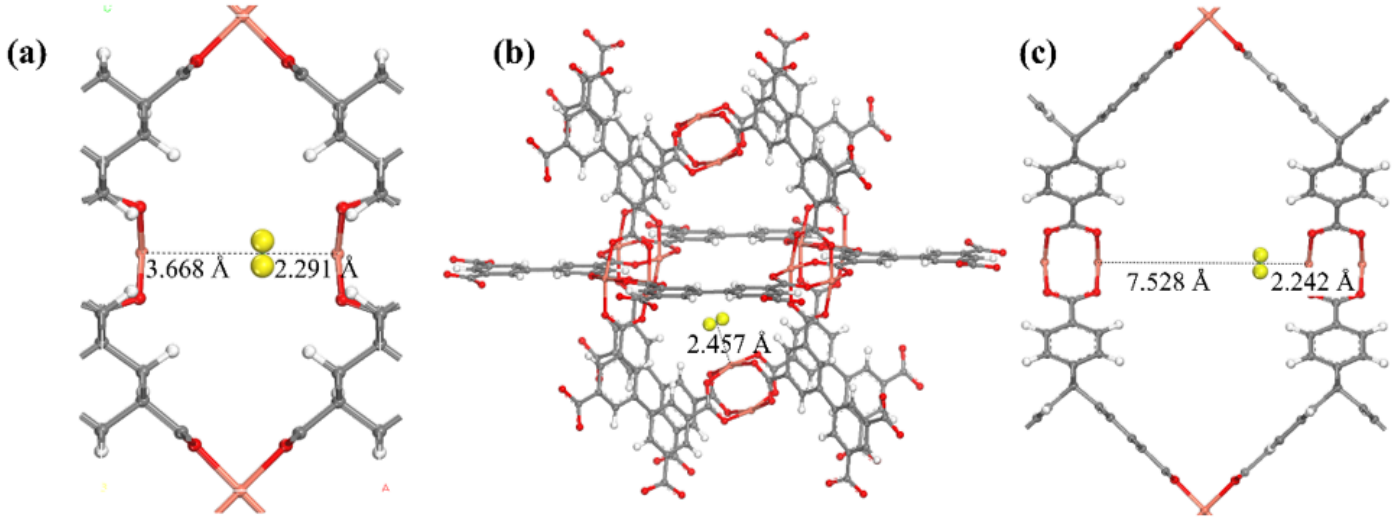

Figure 9

A molecular illustration of the H_2 binding site (a) between the Cu OMSs of adjacent paddlewheels in Cu-ATC and about a single Cu OMS in Cu-bptc (b) and Cu-mbtc (c) as determined from simulation. The adsorbate molecules are shown in yellow.

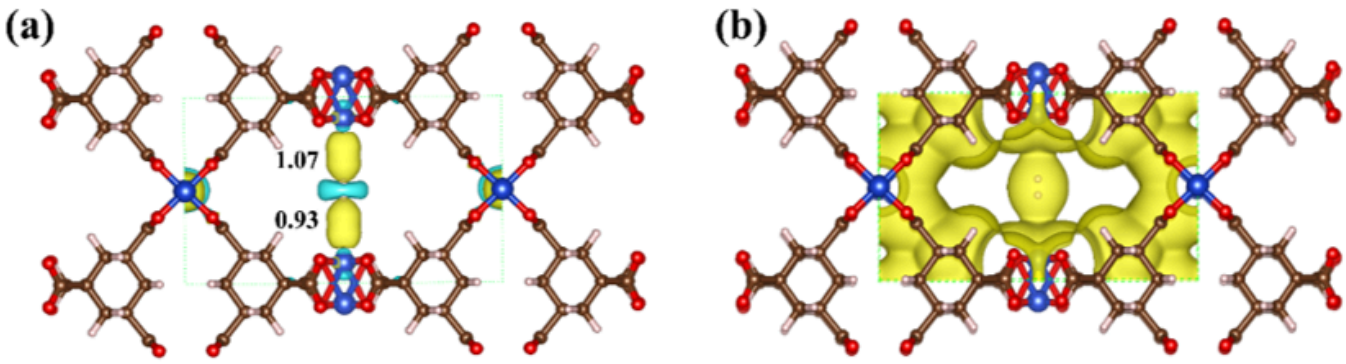

Figure 10

The 3D charge density difference (a) and electron density distribution (b) of Cu-ATC-D_2. The yellow zone and cyan zone denote the charge accumulation and depletion.

Supplementary Files

This is a list of supplementary files associated with this preprint. Click to download.

- Supportinginformation.docx